Biomed Tech 2012; 57:79–87 © 2012 by Walter de Gruyter • Berlin • Boston. DOI 10.1515/bmt-2011-0059

Comparing measured and simulated wave directions in the left atrium – a workflow for model personalization and validation[a]

Michael Burdumy[1,*], Armin Luik[2], Peter Neher[1,3], Raghed Hanna[1,3], Martin W. Krueger[1], Christopher Schilling[1], Hans Barschdorf[3], Cristian Lorenz[3], Gunnar Seemann[1], Claus Schmitt[2], Olaf Doessel[1] and Frank M. Weber[1]

[1] Institute of Biomedical Engineering, Karlsruhe Institute of Technology (KIT), Karlsruhe, Germany
[2] Städtisches Klinikum Karlsruhe, Karlsruhe, Germany
[3] Philips Research Laboratories, Hamburg, Germany

Abstract

Atrial arrhythmias are frequently treated using catheter ablation during electrophysiological (EP) studies. However, success rates are only moderate and could be improved with the help of personalized simulation models of the atria. In this work, we present a workflow to generate and validate personalized EP simulation models based on routine clinical computed tomography (CT) scans and intracardiac electrograms. From four patient data sets, we created anatomical models from angiographic CT data with an automatic segmentation algorithm. From clinical intracardiac catheter recordings, individual conduction velocities were calculated. In these subject-specific EP models, we simulated different pacing maneuvers and measurements with circular mapping catheters that were applied in the respective patients. This way, normal sinus rhythm and pacing from a coronary sinus catheter were simulated. Wave directions and conduction velocities were quantitatively analyzed in both clinical measurements and simulated data and were compared. On average, the overall difference of wave directions was 15° (8%), and the difference of conduction velocities was 16 cm/s (17%). The method is based on routine clinical measurements and is thus easy to integrate into clinical practice. In the long run, such personalized simulations could therefore assist treatment planning and increase success rates for atrial arrhythmias.

Keywords: ablation; atrial fibrillation; electrophysiology; patient-specific models.

[a] This research has been awarded as an excellent contribution to BMT 2010 in Rostock, the annual conference of the German Association of Biomedical Engineering.

* Corresponding author: Michael Burdumy, Institute of Biomedical Engineering, KIT, Kaiserstrasse 12, 76131 Karlsruhe, Germany
Phone: +49-721-60842650
Fax: +49-721-60842789
E-mail: publications@ibt.kit.edu

Introduction

Atrial fibrillation (AF) is a common cardiac arrhythmia that leads to increased morbidity and mortality [4, 15]. At present, AF is often treated by catheter ablation, which has become a routine clinical procedure for symptomatic patients [5, 20, 24]. However, the success rates of the treatment are only moderate and depend highly on the expertise of the clinician [13, 19]. Electrophysiological (EP) modeling and simulation of the heart could help the clinician in planning the procedure and increase the success rates [9]. General models of the heart have been created and validated with respect to average parameters of cardiac anatomy and physiology [8]. For applications regarding diagnosis and therapy of individual patients, however, simulation parameters have to be personalized for each individual [16, 21].

The most important parameters for personalization comprise cardiac anatomy and EP parameters. Conduction velocity (CV) is an especially important parameter because, among others, it determines the wavelength of re-entrant arrhythmias [1, 11, 26]. Furthermore, before drawing clinical conclusions, the pattern of the excitation propagation in the personalized simulation needs to be validated by comparing it to measured data. Different approaches have been taken to personalize EP simulations of the heart [14, 23, 27]. They include a high level of detail but are restricted to *ex vivo* measurements on animal hearts.

In this work, in contrast, we generate and validate personalized human atrial models from standard clinical measurements on AF patients. The presented workflow is based on angiographic computed tomography (CT) scans of the heart and intracardiac electrograms (EGMs) measured with circular mapping catheters (CMCs). From these data, we first create personalized anatomical models. From the intracardiac EGM recordings, we then personalize the CV of the isotropic simulation model. For validation, we reproduce clinical EP measurements in a simulation (*in silico*) considering the recorded clinical stimulus sites and CMC locations. We then compare simulated wave propagation directions to the clinical data and CVs to the clinical data. Our main focus lies on comparing the wave directions with our tested cosine fit algorithm, as it is a fast and easy instrument to validate the created models.

The workflow is applied to four patient data sets. Incidence angles and conduction velocities are presented, and the success of the method is exhibited.

Methods

In our work, we used data sets that were retrospectively acquired from four patients with a mean age of 64±12 years

Table 1 Patient data.

Patient	Age (years)	Sex	AF type	Measurement location
1	50	F	Paroxysmal	LA roof
2	73	F	Paroxysmal	LA post
3	58	M	Paroxysmal	LA roof
4	75	F	Paroxysmal	LA roof

(see Table 1). They had paroxysmal AF and underwent EP study for catheter ablation of the pulmonary veins (PVs) [19]. Before the EP study, an angiographic CT-scan of the left atrium (LA) and the PV ostia was performed. During the EP study, the cardiologist introduced different catheters *via* a right femoral vein access: a 10-electrode CMC (Inquiry Optima; St. Jude Medical, St. Paul, MN, USA) and an ablation catheter (Cool Path Duo; St. Jude Medical, St. Paul, MN, USA) were placed in the LA, and an octopolar catheter (EP-XT, Bard Electrophysiology, Lowell, MA, USA) was placed in the coronary sinus (CS).

The data contained EGMs measured in normal sinus rhythm (NSR) as well as during pacing from different CS catheter bipoles. These EGMs were recorded with the CMC on the LA roof or the LA posterior wall. During the measurements, the catheter was in a stable position.

Measured bipolar EGMs (sampling frequency 1200 Hz) were then retrospectively extracted from the EnSite NavX electroanatomical mapping system (St. Jude Medical, St. Paul, MN, USA) for off-line analysis.

Furthermore, a geometry of the LA was created in the NavX system at the beginning of the study by moving the inserted catheter along the surfaces. This inner surface of the atrium was semiautomatically registered with the angiographic CT-scan. The catheter positions were therefore tracked in the CT coordinate system. The NavX geometry and the catheter position data were also extracted for further analysis. Figure 1A depicts the geometry of the patient 1 data set, including catheter positions and calculated incidence directions (see next paragraph).

Analysis of clinical data

To test the presented workflow, all four clinical patient data sets (see Table 1) were processed.

To extract the activation times from the recorded EGMs, a non-linear energy operator was used [10]. As shown by Nguyen et al. [18], this operator provides a means to analyze intracardiac signals. It marks sections of high frequency and amplitude. The energy E_n of a signal x_n at sample n is determined by

$$E_n = x_n^2 - x_{n+1}x_{n-1}. \tag{1}$$

A Gaussian low-pass filter was applied to the operator output. The barycenter of the filtered signal was determined, representing the activation time of the signal. The barycenter was used because it is associated with the spatial point between two electrodes.

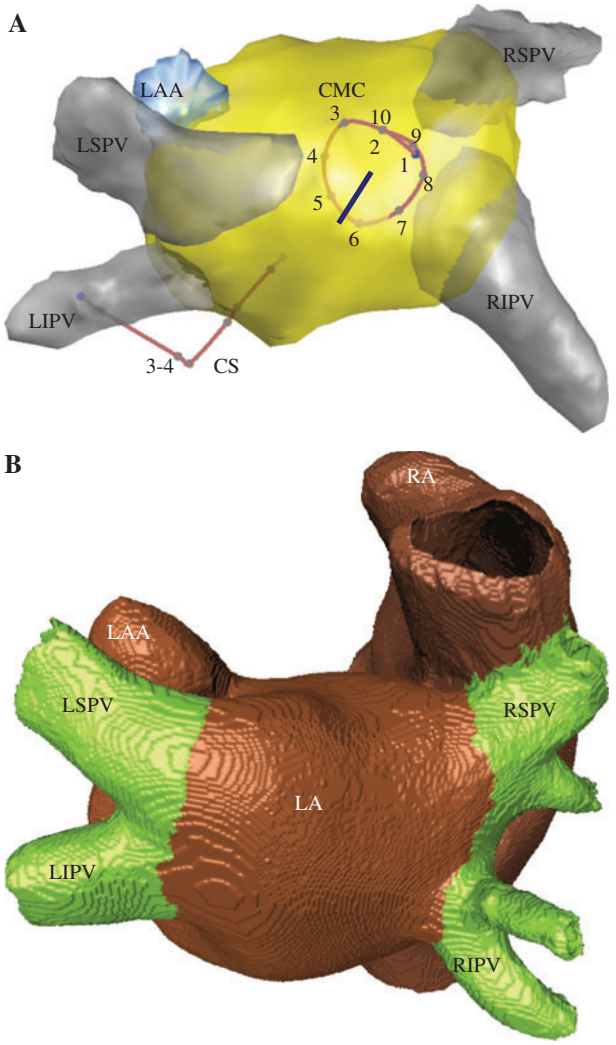

Figure 1 Atrial models of patient 1. (A) Clinical NavX geometry of the LA. Position of CS catheter and CMC catheter during CS 3–4 stimulation. The calculated incidence direction is given by the black line (see results). (B) Voxel model of the automatically segmented atria. The colors represent the different tissue properties that were used in the CA: LA, RA, and LA auriculum are brown; distal parts of the inferior and superior PVs (left and right, thus, e.g., left inferior PV) are green.

For the purpose of our analysis we assume that a plane excitation wavefront travels across the CMC. A quantitative method as described by Weber et al. [30] was used to analyze a complete activation pattern derived from the whole set of catheter electrodes, where the pattern $t(n)$ can be described by the cosine function

$$t(n) = t_c - A \cdot \cos[\gamma(n\text{-}1) - \varphi_0]. \tag{2}$$

Figure 1B shows the voxelized atrial model of the automatically segmented CT data of patient 1.

Parameter $t(n)$ describes the activation time of the n^{th} electrode, with activation times from bipolar signals assigned to half-integer numbers (1.5, 2.5, …). The mean activation time t_c corresponds to the base line of the cosine function, and

φ_0 marks the angle at which the first activation occurs. The parameter γ describes the angle offset between two neighbor electrodes and depends on the geometry and electrode spacing of the catheter (typically 30°–40°).

The parameters t_c, A, γ, and φ_0 were fitted to any detected set of activation times, with initial values and boundaries estimated from the activation sequence.

The incidence direction of the wave propagation was given by φ_0. In addition, the CV could be calculated from the cosine amplitude and the catheter radius. The catheter radius was recalculated for each activation time from the mapped position data to account for possible changes during the examination.

Presentation of the workflow used

Figure 2 demonstrates the structure of our applied workflow. Intracardiac EGMs were recorded under different pacing conditions. For each recorded wavefront, the CV and direction of the wave propagation were determined. A CT image set of the patient's thorax was automatically segmented to obtain an anatomical model of the atria (see Automatic segmentation method section). Excitation was simulated in this model with an adaptive cellular automaton (CA; see CA in the Voxelized atrial model section) that used the determined CV values. From the resulting transmembrane voltages, the extracellular potential distribution was calculated, and the potentials were extracted at the positions of the clinical CMC electrodes (Forward calculation in a tetrahedral mesh of the atrium section). For the clinical data, the synthetic signals were analyzed with the same algorithm as presented in the section Analysis of clinical data. The resulting wave directions and CVs were compared to results from the clinical data (Comparison of clinical and simulated EGM measurements section).

Automatic segmentation method

Standard clinical angiographic CT-scans with resolutions 0.69×0.69×1 mm (patients 1, 2, 4) and 0.69×0.69×3 mm (patient 3) were available. The timing of the CT-scan was performed such that the contrast agent was mainly located in the LA and the PVs. The atria were segmented from the CT image slices using an automatic segmentation algorithm developed at Philips Research Hamburg [6, 17]. A brief summary is given in the following.

First, a mean model of the whole heart was adapted to the patient CT-scan. This provided a rough position reference to insert more detailed separate left and right atrial models. To cope with the topological organ variability of the PVs in the LA, a hybrid method was used, using both region growing and model-based segmentation [6]. In the region of highest

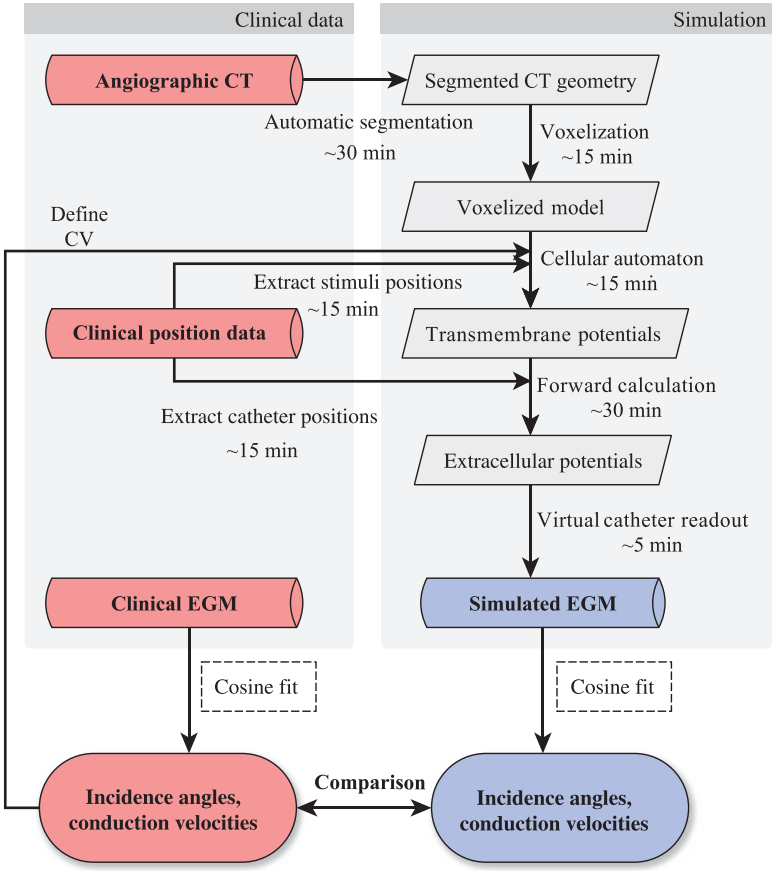

Figure 2 Diagram of the workflow for generation and validation of personalized EP simulations. The given times correspond to the time needed for the completion of one step using a standard PC (here, a single core of an Intel Core 2 Duo, 2×2.8 GHz).

topological variability, a guided, topology-sensitive region growing was applied. It determined the number (and early bifurcations) of PVs, identifying the given anatomical variant (see Figure 3). Based on this information, one of three surface models was selected and adapted to the target object. The three surface models featured one, two, and three right PVs.

Next, according to the selected LA model, a complete mesh of both atria was chosen [17]. This mesh had nine differently labeled regions. These regions were assigned different parameters for further adaptation. The most important parameters were the allowed range of the image gradient feature, the maximum feature search distance, the weighting of the external energy as well as a feature distance penalty. In a number of iteration steps, the parameters were automatically changed to best fit the CT data. Last, a precalculated tetrahedral mesh with specific, rule-based wall thickness was transformed using the same parameters. The transformation was done with a thin plate splines approach [17]. The precalculated tetrahedral meshes also included information on the location of special propagation pathways (e.g., Bachmann bundle, terminal crest, sinus node). As a first approximation, however, all propagation pathways were treated as normal myocardium in this work.

CA in the voxelized atrial model

The voxelized geometry of the patient's heart was taken as input for an adaptive CA [31], which was used to simulate electrical excitation propagation. The CA was parameterized from the atrial cell model by Courtemanche et al. [3]. Each cell of the CA can adopt different states depending on its history and conduct its excitation to a cell of the neighborhood.

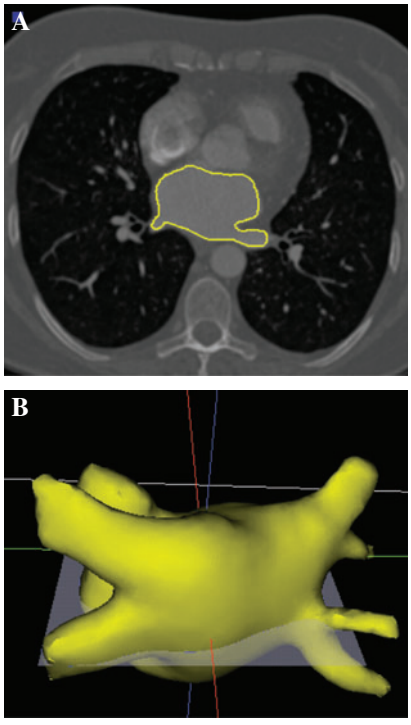

Figure 3 Patient 1 – automatic segmentation of LA. (A) Transversal slice of the angiographic CT data set. The automatically segmented LA is displayed by a yellow line. (B) Three dimensional model of the segmented LA. The picture on the left was taken from the indicated layer.

Because the automaton is rule-based, the absolute CV value for each tissue can be directly set and is independent of, e.g., wavefront or tissue curvature. The voxelized model adopted three different regions from the automatic segmentation: LA, right atrium (RA), and distal PVs. Additionally, the position of the sinus node was used for stimulation in the NSR cases. The CV of the LA was set to a personalized value in each simulation, depending on the calculated mean CVs from the respective clinical measurements. The patient-specific CV values are given in Table 2. Because no measurements were available from the RA, it was assigned a constant CV of 70 cm/s (within the range reported by Hansson et al. [7]). The PV ostia were simulated with the same parameters as the LA myocardium, and the distal PVs were set to be non-conductive. It must be emphasized that in the current isotropic setup, the CV does not change the order in which the voxels are activated and thus does not affect the simulated incidence directions.

For each patient, up to three different stimulation sites were considered: the sinus node (for NSR) and two positions in the CS (CS 3–4 and CS 7–8). The stimulation center for the simulation of the CS pacing was extracted from the recorded NavX positions. As this site was located outside of the myocardium, an algorithm was used that calculated the closest point of the myocardial surface of the voxel model to the stimulation source. The position of the sinus node was determined by the automatic segmentation and was taken as stimulation source for our NSR simulations. In each setup, the CA was initialized with four beats at a cycle length of 500 ms. The transmembrane voltages of the fifth beat were then recorded at a time resolution of 1 ms.

Forward calculation in a tetrahedral mesh of the atrium

To calculate extracellular potentials on the heart surface, a finite element forward calculation was done. From the voxel model of the CA, a tetrahedral mesh was generated. To this end, the atrium was placed in a surrounding blood environment. In the forward calculation, the bidomain approach was used to compute extracellular potentials on the heart surface [22]. The maximum size of the tetrahedral finite elements was set to 0.8 mm.

In these forward calculations, the potentials needed to be extracted at sites corresponding to the catheter positions in the clinical measurements, defined by the navigation system. However, the LA wall in the geometry calculated by the NavX system could be shifted by several millimeters compared to the segmented CT geometry. Without further correction, electrode positions from the mapping system could therefore correspond to points in the simulation model that were located in the blood, inside the heart tissue, or outside the atrium. Because the electrodes of the measuring CMC had to lie on

Table 2 Results of the cosine fit algorithm.

Patient	Stimulus site	Duration (s)	Direction φ (°)			CV (cm/s)			
			Clinical	Simulated	Δ	Clinical	Simulated	Δ_{abs}	Δ_{rel} (%)
1	CS 3–4	9	211±4	224	13	70±4	69	-1	-2
	CS 7–8	8	268±20	255	-13	109±8	103	-6	-5
	(NSR)	13	51±6	25	-26	108±2	118	9	8
2	CS 3–4	21	176±2	169	-7	83±9	91	8	10
	(NSR)	91	316±23	325	9	56±6	78	22	39
3	CS 3–4	11	29±7	38	8	96±8	81	-15	-16
	CS 7–8	16	18±15	23	4	103±4	134	31	30
	(NSR)	28	227±7	246	20	125±7	99	-26	-21
4	CS 3–4	16	103±9	93	-10	93±8	72	-21	-22
	CS 7–8	11	83±3	119	36	81±9	65	-16	-20
	(NSR)	11	271±1	287	16	100±8	82	-18	-18
Mean (over absolute values)						15±9	(8%)	16±9	(17%)

CMC measuring site: roof or posterior wall of the LA.

the inner surface of the heart, the positions were projected onto the surface along the normal direction of the catheter plane with an established algorithm [29].

The impedance-based position mapping of the electrodes [32] assumes homogeneous field distributions in the thorax. Field inhomogeneities can lead to distortions in the recorded catheter geometry, such as a more oval catheter shape. Such oval shapes were recorded in patients 2–4, although sporadic comparisons to fluoroscopic images did not indicate such a deformation. However, as a first approximation, the recorded oval catheter geometry was inserted into the simulation model without further corrections.

Furthermore, in patient 3, the recorded CMC geometry was not parallel to the surface. In this case, projection along its normal $\vec{n}_c$ would have led to a wrong position of the catheter. To ensure a correct positioning, the CMC was rotated around its center with the rotation axis $\vec{n}_r$ determined by

$$\vec{n}_r = \vec{n}_s \cdot \vec{n}_c, \tag{3}$$

such that the surface normal $\vec{n}_s$ and the new catheter normal were parallel. This way, the CMC was not rotated around the axes perpendicular to its plane to avoid artificial offsets in the incidence angle.

In the tetrahedral model, the electrodes were modeled as metallic spheres with a radius of 1 mm. From the signals at the electrode centers, the bipolar EGMs could then be calculated.

Comparison of clinical and simulated EGM measurements

To validate the quality of our simulations, we compared the directions of the excitation waves from the clinical data with the corresponding simulated data. This was accomplished by analyzing the bipolar electrode measurements at the virtual catheter positions and the EGMs recorded in the clinic with the cosine fit algorithm. With this comparison, it could be estimated how well the simulated local excitation pattern matched the local excitation pattern in the patient.

Additionally, the CV that was calculated from the simulations by the cosine fit was compared to the patient-specific CV specified in the CA. However, this was not an actual model validation with respect to clinical measurements. It was rather an estimation of how exactly the known CV in the simulation could be determined with the *in silico* measurement. Higher deviations in the compared CVs could stem from errors in the navigation system or from catheter deformations in the catheter placement procedure. Thus, the comparison of CVs validates the model generation process itself, whereas the comparison of incidence angles confirms the ability of the model to mimic physiological measurements.

Results

Results of the automatic segmentation and positioning of the electrodes

All CT data sets could be segmented into detailed models with a voxel size of 0.33 mm. The models featured regionally different wall thickness and exhibited a smooth surface. When viewed in combination with the original image data, the segmented PVs followed the anatomical structures closely; thus, the models with the right amount of PVs were chosen. With a resolution of 0.33 mm, the automatic segmentation had a much higher level of detail than the geometry from the clinical navigation system. All positions of the CMC, taken from the navigation system, could be inserted into the detailed geometry, thus validating the registration of both geometries. In patient 4, the CMC had to be rotated to be aligned with the surface. It could be noted that in patients 2–4, NavX recorded an oval shape of the CMC that was transferred into the simulation.

Figure 3A displays a CT slice of patient 1, including the automatically segmented LA surface, whereas Figure 3B depicts the whole three-dimensional surface model.

Comparison of clinical measurements to simulation results

Table 2 provides an overview of the results from all simulations. For the interpretation of the angle differences, the distance between two neighboring electrodes of around 40° is a good reference. Angles that differed by <1 electrode distance were considered to show good correspondence with the clinically measured direction. The total angular difference between corresponding calculations from the clinic and simulations was 15°±9°, and the total difference of the CV was 16±9 cm/s (17%).

The absolute angle difference of patient 1 during both CS stimulations was 13°; during NSR, it was slightly higher with 26°. The CV showed little difference when comparing the manually set and calculated velocities. Errors ranged from 1 to 9 cm/s.

Figure 4A depicts a simulated wavefront during pacing from CS electrodes 3–4. The CV of the tissue was set to 70 cm/s, the mean value determined from the clinical data during CS 3–4 pacing (see Table 2).

In the case depicted in Figure 4A, the calculated incidence directions differed by <15°, which compares to roughly half an electrode distance. The figure shows that if the clinical angle was not known, the simulated angle could provide a useful estimate on the origin of the wavefront. The shape of the projected virtual catheter closely resembles a circle. As pointed out before, the CV differed by <5 cm/s.

Figure 4B depicts the difference signals recorded by the CMC during the clinical measurements and the simulated signals at corresponding locations from the EP simulations. It can be seen that, in both cases, the earliest peak appears in electrodes 5–6. Therefore, these are the electrodes that the excitation wavefront reaches first. The fitted cosine line has the same morphology in both cases, which is why angle and CV calculation yield accurate values.

Patient 2's data set did not provide a stimulation from the CS 7–8 electrodes. For NSR and CS 3–4 stimulation, however, the angles and velocities from clinic and simulation showed good agreement (see Table 2).

For the stimulation cases, the angle differences for patient 3 were 8° and 4° and again higher at NSR with 20°. The differences in the CVs were considerably higher than, e.g., in patient 1's case.

The angle difference in the CS 3–4 case of patient 4 was 10°; in the CS 7–8 case, 36°, the highest difference. In clinical measurements the incidence angle at CS 3–4 was higher than at CS 7–8. The simulations show switched results, here the incidence angle at CS 7–8 was higher than at CS 3–4. This discrepancy may be due to the fact that in certain areas of the atrium conduction behaves differently than our simple model expects. Further customization, such as the inclusion of conduction pathways, fiber orientations, and also a more exact positioning systems might improve the results (see Benefits and drawbacks of the workflow section).

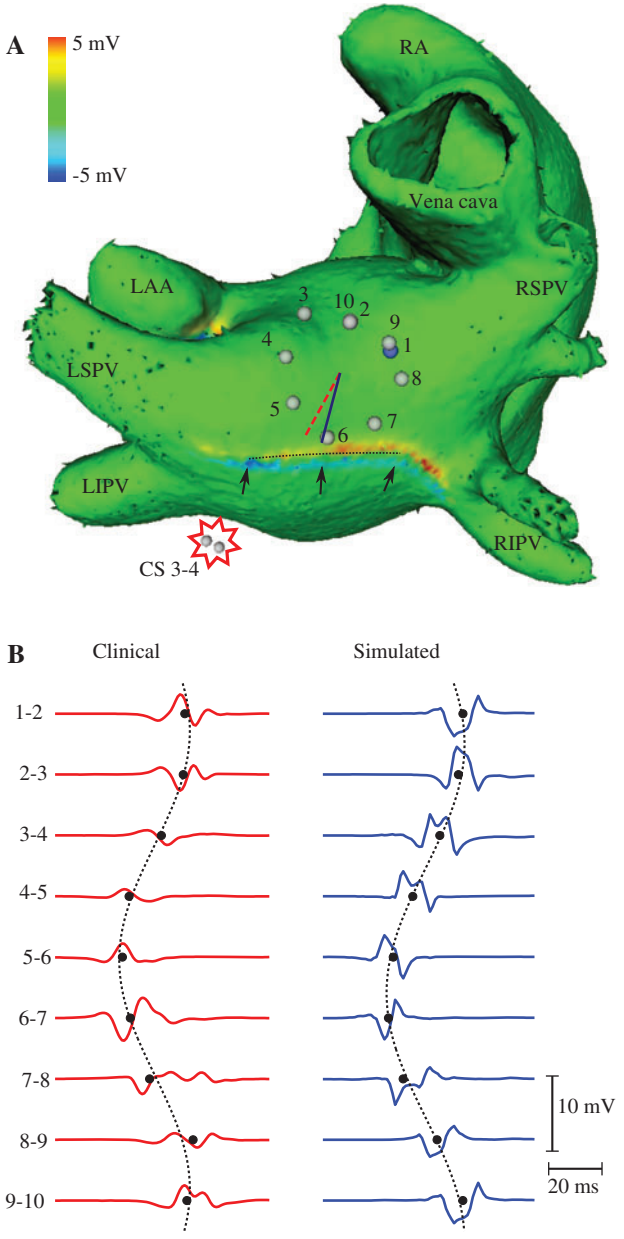

Figure 4 Patient 1 during CS 3–4 stimulation – simulated wavefront and EGMs from clinical measurement and simulation. (A) Simulated wavefront on the segmented geometry 58 ms after excitation (extracellular potential color coded). The red dashed line depicts the incidence angle from the clinical measurements; the blue line is calculated from the simulation. Stimulation originated in the CS 3–4 electrodes, depicted at the bottom of the atrium. The electrodes are located on the endocardial surface, but for viewing purposes, they are depicted on the outer surface of the atrium. (B) Clinically measured (left) and simulated (right) EGM. The non-linear energy operator determines the times, displayed by black dots, onto which a cosine is fitted (dotted line).

Discussion

In our work, we have presented a workflow for the generation of subject-specific atrial simulations and their validation by comparing incidence angles and conduction velocities. It is based on routine clinical data and adds no additional burden to the patient. The workflow includes automatic segmentation of the atria, a CA, and calculation of extracellular potentials after excitation. This way, typical EP studies can

be reproduced *in silico*, i.e., in the computer model. Due to coregistration of the computer model and projected catheter positions that were taken from clinical measurements, we could imitate clinical activation patterns in our simulations. A previously reported cosine fit algorithm [29] was applied to calculate wave directions and conduction velocities using the position and EGMs from the clinical and simulated data. Results from both of these were compared.

Overall, the average difference between simulated and clinical incidence angles was 15° or, relative to a half circle of 180°, 8%. For model validation, this presents fully satisfactory results considering the simplicity of the model. It shows that even without inclusion of propagation pathways and fiber orientation, excitation conduction in the patients at the measurement locations could be well reproduced.

Furthermore, the models could be personalized with individual conduction velocities. When reproducing the CV measurements in the model, the average CV difference was 16 cm/s, or 17%. The conduction velocities of patients 2–4 displayed higher deviation than the velocities from patient 1. Here, it could be seen that the oval deformation in the catheter position data caused a "real" deformation in the simulation catheter. This did not affect angle calculation, as the cosine fit always assumes a circular shape of the catheter. It did, however, affect the velocity calculation. Here, given a more oval shape of the CMC, a propagating wave would pass one direction faster than the one perpendicular to it. The cosine fit, however, always assumes a circular shape of the catheter. Thus, depending from which direction the wavefront travels across the catheter, different velocities are calculated that in turn may lead to higher errors in the velocity comparison.

All processing steps were performed on a single core of an Intel Core 2 Duo desktop processor (2×2.8 GHz). The total time needed to conduct an initial simulation was approximately 2 h (see Figure 2). Further simulations with the same patient data were much faster and could be run simultaneously, as most of the data, such as the segmented voxel model, only had to be calculated once. Without optimizations, this is already within the time span that is available for possible clinical applications. Further optimizations (such as, e.g., the parallelization of different forward calculation time steps) could speed up the process even more.

Benefits and drawbacks of the workflow

As an example, Relan et al. [23] also presented a workflow for personalization of cardiac EP simulations of the ventricles. The group used diffusion tensor magnetic resonance imaging and optical mapping data from *ex vivo* porcine hearts to generate subject specific models. Therefore, their models provide a higher level of detail, especially regarding conduction pathways and fiber orientation, that is not given in our study. However, for such an approach, all data must be acquired with *ex vivo* methods or has to be integrated *via* previous knowledge from *ex vivo* findings. This is not possible in the case of human personalization. The great benefit of our presented method is that there is a huge amount of data recorded every day in clinical catheter laboratories that could be analyzed with such an efficient workflow.

As can be seen from the simulated and clinical EGMs in Figure 4B, the morphology and polarity of several channels differ. This could stem from the simple approach using the CA. On the other hand, the simulated signals are ideal signals. In clinical settings, many factors, such as wall contact, contact pressure, or tissue impedance may influence the signal.

The rule-based excitation simulations with the CA could be replaced by detailed EP cell models coupled with the monodomain or bidomain approach [22]. Atrial cell models contain detailed descriptions of ionic membrane currents for physiological cases and AF patients [3, 25]. Furthermore, phenomenological cell models can be adapted to reproduce specific excitation and restitution properties [2, 28]. For these simulations, the voxelized model of the segmented atrial geometry is not restricted to a voxel size of 0.33 mm. Higher resolutions (e.g., 0.2 mm) can easily be generated for simulations with a higher level of detail. However, the increase in precision would come at the expense of speed and simplicity.

Both navigation system and the applied projection method gave oval shapes of the catheter. As mentioned in the preceding paragraph, it needs to be investigated whether a different projection method that forces circular shapes of the virtual catheter leads to better results (compare findings of Weber et al. [30] for simulated measurements with a circular catheter on the LA roof, where the error was around 1.5% only).

In our model, conduction in the different tissues was assumed to be homogeneous. It is probable that directional propagation pathways, such as directional muscle fibers, could be responsible for the angle difference in our CS stimulations. Future models of the atria could include fiber orientation and further improve excitation simulations [12]. The inclusion of special fast propagation pathways, such as the Bachmann bundle and terminal crest in an NSR test setup yielded only marginal changes in the calculated angle, which is why they were left out in our study. However, the systematic study of conduction anisotropies might reveal stronger effects for certain cases. Furthermore, anatomically varying position of the sinus node in our patients could lead to different wave directions in clinical measurements and simulations.

Our method is not restricted to stimulations from the sinus node or CS catheter. The setup gives free choice in the stimulus location. However, up to now the cosine fit algorithm restricts the shape of the catheter to be circular and can only calculate incidence directions for plane wavefronts, which limits the measurement regions to large and homogenous areas of the atrium. In the future, other catheter shapes, e.g., spirals or PentaRay catheters, can be possibly included. With appropriate analysis techniques, even complex activation patterns, such as multiple and simultaneous stimulations could be analyzed and compared. In future studies, our workflow and the CA could be used to generate an initial simulation model that is then further refined using above-mentioned detailed cell models, fiber orientations, and fast conduction pathways. The wealth of clinical data that are recorded in catheter laboratories everyday could help to train and improve these refined models.

Conclusions

By successfully applying our workflow to four different patient data sets, we demonstrated the efficiency and ease of use of our method. The analysis of data from clinical ablation procedures is an ongoing process. The more patient data are analyzed, the more information can be acquired on excitation and propagation of wavefronts in healthy and pathological atria. In parallel, the functionality of the workflow and the simulation will improve. The herein presented results were overall very good and represent one step further toward clinically usable personalized EP models.

Acknowledgments

The work of F. M. Weber was supported by Philips Research, Hamburg. The work of M. W. Krueger was supported by the European Community's Seventh Framework Programme (n224495, "euHeart Project").

References

[1] Allessie M, Bonke F, Schopman F. Circus movement in rabbit atrial muscle as a mechanism of trachycardia. III. The "leading circle" concept: a new model of circus movement in cardiac tissue without the involvement of an anatomical obstacle. Circ Res 1977; 41: 9–18.

[2] Bueno-Orovio A, Cherry E, Fenton F. Minimal model for human ventricular action potentials in tissue. J Theor Biol 2008; 253: 544–560.

[3] Courtemanche M, Ramirez RJ, Nattel S. Ionic mechanisms underlying human atrial action potential properties: insights from a mathematical model. Am J Physiol 1998; 275: H301–H321.

[4] Fuster V, Ryden LE, Cannom DS, et al. ACC/AHA/ESC 2006 guidelines for the management of patients with atrial fibrillation: a report of the American College of Cardiology/American Heart Association task force on practice guidelines and the European Society of Cardiology committee for practice guidelines (writing committee to revise the 2001 guidelines for the management of patients with atrial fibrillation): developed in collaboration with the European Heart Rhythm Association and the Heart Rhythm Society, 2006.

[5] Haissaguerre M, Jais P, Shah DC, et al. Spontaneous initiation of atrial fibrillation by ectopic beats originating in the pulmonary veins. N Engl J Med 1998; 339: 659–666.

[6] Hanna R, Barschdorf H, Klinder T, et al. A hybrid method for automatic anatomical variant detection and segmentation. In: Metaxas D, Axel L, editors. FIMH 2011, LNCS 6666, 2011: 333–340.

[7] Hansson A, Holm M, Blomstrom P, et al. Right atrial free wall conduction velocity and degree of anisotropy in patients with stable sinus rhythm studied during open heart surgery. Eur Heart J 1998; 19: 293–300.

[8] Harrild DM, Henriquez CS. A computer model of normal conduction in the human atria. Circ Res 2000; 87: e25–e36.

[9] Jacquemet V, Kappenberger L, Henriquez C. Modeling atrial arrhythmias: impact on clinical diagnosis and therapies. IEEE Rev Biomed Eng 2008; 1: 94–114.

[10] Kaiser JF. On a simple algorithm to calculate the 'energy' of a signal. Proc. IEEE Int. Conf. Acoust. Speech Signal Process. 1990: 381–384.

[11] Kleber A, Rudy Y. Basic mechanisms of cardiac impulse propagation and associated arrhythmias. Physiol Rev 2004; 84: 431–488.

[12] Krueger MW, Schmidt V, Tobón C, et al. Modeling atrial fiber orientation in patient-specific geometries: a semi-automatic rule-based approach. In: Metaxas D, Axel L, editors. FIMH 2011, LNCS 6666 2011: 223–232.

[13] Luik A, Merkel M, Riexinger T, Wondraschek R, Schmitt C. Persistent atrial fibrillation converts to common type atrial flutter during CFAE ablation. Pac Clin Electrophysiol 2010; 33: 304–308.

[14] MacLeod RS, Stinstra JG, Lew S, et al. Subject-specific, multiscale simulation of electrophysiology: a software pipeline for image-based models and application examples. Philos Trans R Soc A Math Phys Eng Sci 2009; 367: 2293–2310. DOI 10.1098/rsta.2008.0314.

[15] Nattel S. New ideas about atrial fibrillation 50 years on. Nature 2002; 415: 219–226.

[16] Neal M, Kerckhoffs R. Current progress in patient-specific modeling. Brief Bioinform 2010; 11: 111.

[17] Neher P, Barschdorf H, Dries S, et al. Automatic segmentation of cardiac CTS – personalized atrial models augmented with electrophysiological structures. In: Metaxas D, Axel L, editors. FIMH 2011, LNCS 6666 2011: 80–87.

[18] Nguyen MP, Schilling C, Dössel O. A new approach for automated location of active segments in intracardiac electrograms. IFMBE Proc World Congr Med Phys Biomed Eng 2009; 25: 763–766.

[19] Oral H, Knight BP, Ozaydin M, et al. Segmental ostial ablation to isolate the pulmonary veins during atrial fibrillation: feasibility and mechanistic insights. Circulation 2002; 106: 1256–1262.

[20] Pappone C, Rosanio S, Oreto G, et al. Circumferential radiofrequency ablation of pulmonary vein ostia: a new anatomic approach for curing atrial fibrillation. Circulation 2000; 102: 2619–2628.

[21] Plank G, Burton RAB, Hales P, et al. Generation of histoanatomically representative models of the individual heart: tools and application. Philos Trans A Math Phys Eng Sci 2009; 367: 2257–2292.

[22] Pullan AJ, Buist ML, Cheng LK. Mathematically modelling the electrical activity of the heart: from cell to body surface and back again. Singapore: World Scientific 2005.

[23] Relan J, Pop M, Delingette H, Wright GA, Ayache N, Sermesant M. Personalization of a cardiac electrophysiology model using optical mapping and MRI for prediction of changes with pacing. IEEE Trans Biomed Eng 2011; 58: 3339–3349. DOI 10.1109/TBME.2011.2107513. ISSN 0018-9294.

[24] Schmitt C, Deisenhofer I, Zrenner B, editors. Catheter ablation of cardiac arrhythmias: a practical approach. Steinkopff, Darmstadt, Germany: Springer 2006. ISBN 3-7985-1575-1.

[25] Seemann G, Carrillo Bustamante P, et al. Atrial fibrillation-based electrical remodeling in a computer model of the human atrium. Proc Comput Cardiol 2010; 37: 417–420.

[26] Smeets JL, Allessie MA, Lammers WJ, Bonke FI, Hollen J. The wavelength of the cardiac impulse and reentrant arrhythmias in isolated rabbit atrium. The role of heart rate, autonomic transmitters, temperature, and potassium. Circ Res 1986; 58: 96–108.

[27] Vigmond E, Vadakkumpadan F, Gurev V, et al. Towards predictive modelling of the electrophysiology of the heart. Exp Physiol 2009; 94: 563.

[28] Weber FM, Lurz S, Keller DUJ, et al. Adaptation of a minimal four-state cell model for reproducing atrial excitation properties. Proc Comput Cardiol 2008; 35: 61–64.

[29] Weber FM, Schilling C, Straub D, et al. Extracting clinically relevant circular mapping and coronary sinus catheter potentials from atrial simulations. LNCS 2009; 5528: 30–38.
[30] Weber FM, Schilling C, Seemann G, et al. Wave direction and conduction velocity analysis from intracardiac electrograms – a single-shot technique. IEEE Trans Biomed Eng 2010; 57: 2394–2401.
[31] Werner CD, Sachse FB, Dössel O. Electrical excitation propagation in the human heart. Int J Bioelectromagn 2000; 2. http://ijbem.k.hosei.ac.jp/volume2/number2/werner/paper_ijbem.htm.
[32] Wittkampf FH, Wever EF, Derksen R, et al. LocaLisa: new technique for real-time 3-dimensional localization of regular intracardiac electrodes. Circulation 1999; 99: 1312–1317.

Received May 26, 2011; accepted January 5, 2012; online first February 22, 2012